RESEARCH ARTICLE

Macromolecular Rapid Communications
www.mrc-journal.de

Tuning the Internal Compartmentation of Single-Chain Nanoparticles as Fluorescent Contrast Agents

*Justus F. Thümmler, Andreas H. Roos, Jana Krüger, Dariush Hinderberger, Franz-Josef Schmitt, Guo Tang, Farzin Ghane Golmohamadi, Jan Laufer, and Wolfgang H. Binder**

Controlling the internal structures of single-chain nanoparticles (SCNPs) is an important factor for their targeted chemical design and synthesis, especially in view of nanosized compartments presenting different local environments as a main feature to control functionality. We here design SCNPs bearing near-infrared fluorescent dyes embedded in hydrophobic compartments for use as contrast agents in pump–probe photoacoustic (PA) imaging, displaying improved properties by the location of the dye in the hydrophobic particle core. Compartment formation is controlled via single-chain collapse and subsequent crosslinking of an amphiphilic polymer using external crosslinkers in reaction media of adjustable polarity. Different SCNPs with hydrodynamic diameters of 6-12 nm bearing adjustable label densities are synthesized. It is found that the specific conditions for single-chain collapse have a major impact on the formation of the desired core–shell structure, in turn adjusting the internal nanocompartments together with the formation of excitonic dye couples, which in turn increase their fluorescence lifetime and PA signal generation. SCNPs with the dye molecules accumulate at the core also show a nonlinear PA response as a function of pulse energy—a property that can be exploited as a contrast mechanism in molecular PA tomography.

1. Introduction

Single-chain nanoparticles (SCNPs) are nanostructured, enzyme-like particles that are made of a single polymer chain collapsed and intramolecularly crosslinked either covalently or non-covalently. The countless possibilities of chemical functionalities, synthetic routes, and unique nanostructures enable their use in modern research, like (enzyme like) catalysis,[1] antifouling,[2] or biomedical applications.[3] Their internal structures allow the embedding of functional units like fluorescent dyes in specific regions inside these particles.[4] Choice of the polymer backbone embeds biocompatibility[5] or degradability,[6] changes in the polymer's architecture[7] and the use of crosslinkers for specific covalent or non-covalent collapse reaction types[8] as well as the collapse medium are main factors to reach compartments inside a SCNP.[9]

There are only few reports on a precise control of nanosized compartments inside SCNPs, as they are dynamic entities before and even during the crosslinking process. The formation of compartmented SCNPs[7a] using grafted tri-block copolymers of ABC and ACB type as precursors has been described, displaying differential miscibilities where block A and C are compatible with each other, but block B is compatible with neither. Collapse into SCNPs was accomplished by core crosslinking via photodimerization of cinnamic acid side chains, in turn proving the formation of discrete A, B, and C domains inside the SCNPs. It was shown that the correct choice of both, the surrounding medium of collapse and the crosslinker have a major influence on the SCNP's shape, highlighting the importance of precollapsing the precursor polymer in a poor solvent before the actual crosslinking reaction to yield more globular shaped particles.[10] Both, pre-collapsing and the use of long crosslinkers cause long-range crosslink loops that result in more compact and globular nanoparticles. A similar behavior was found via photocrosslinking a purely hydrophobic polymer either in THF, in hexane, or mixtures of both, resulting in differently dense particles with variable crosslink densities, thus proving the compartmentation of the precursor polymer already in the collapse medium.[11]

In our previous work[12] we have demonstrated the formation of compartmented core–shell structured SCNPs by single-chain

J. F. Thümmler, W. H. Binder
Macromolecular Chemistry, Institute of Chemistry, Faculty of Natural Science II (Chemistry, Physics and Mathematics)
Martin Luther University Halle-Wittenberg
von-Danckelmann-Platz 4, D-06120 Halle, Germany
E-mail: wolfgang.binder@chemie.uni-halle.de

A. H. Roos, J. Krüger, D. Hinderberger
Physical Chemistry, Institute of Chemistry, Faculty of Natural Science II (Chemistry, Physics and Mathematics)
Martin Luther University Halle-Wittenberg
von-Danckelmann-Platz 4, D-06120 Halle, Germany

F.-J. Schmitt, G. Tang, F. G. Golmohamadi, J. Laufer
Institute of Physics, Faculty of Natural Science II (Chemistry, Physics and Mathematics)
Martin Luther University Halle-Wittenberg
von-Danckelmann-Platz 3, D-06120 Halle, Germany

The ORCID identification number(s) for the author(s) of this article can be found under https://doi.org/10.1002/marc.202200618

DOI: 10.1002/marc.202200618

collapse of an amphiphilic polymer in an aqueous crosslinking medium. The hydrophobic crosslinking groups were located at the particle core with a size of 1-2 nm while the hydrophilic PEG side chains formed a water-soluble shell. By covalently binding either a fluorescent or a radical label to unreacted crosslinking sites, we were able to prove their location at the core via fluorescence and electron-paramagnetic-resonance spectroscopy.[12a] The hydrophobic core was still swollen with water molecules, depleted by increasing the temperature.[12b] Different properties of the individual compartments could be proven since the core and shell displayed largely different cloud point temperatures.

In this study, we demonstrate the controlled formation of different nanosized compartments in amphiphilic single-chain nanoparticles by collapsing in different reaction media to specifically embed and protect a fluorescent dye for application in photoacoustic (PA) measurements. The embedding into such compartments is expected to result in enhanced photophysical properties in aqueous solution, such as significantly enlarged fluorescence lifetimes, as the dye molecules are then located in the nonpolar, nanosized compartments able to form excitonic couples, undisturbed by the aqueous surrounding. Furthermore, the embedding into such SCNPs with hydrodynamic diameters of ≈10 nm should be advantageous for the dye's biodistribution and for tissue specific targeting, making the labeled SCNPs good candidates as contrast agents for biomedical applications. We are using the copper catalyzed azide/alkyne click reaction (CuAAC) in either water or in THF using external bivalent crosslinkers for single-chain collapse to effect the formation of compartments. Several spectroscopic methods are used, such as continuous wave electron-paramagnetic-resonance (CW EPR) spectroscopy, standard and time resolved fluorescence spectroscopy, and photoacoustic (PA) pump–probe spectroscopy, a method that exploits long lived excited states in fluorophores.[13] The near-infrared fluorescent dye aza-BODIPY is exploited as a crosslinker due to its optical properties being strongly dependent on the local environment,[12a] thus paving the way toward a targeted design of dye-encapsulating SCNP contrast agents for optical and PA imaging.

2. Results and Discussion

2.1. Polymer and Single-Chain Nanoparticle Synthesis

The first step in the design of compartmented SCNPs is the chemical synthesis of the polymeric precursor bearing the desired amphiphilicity, coupled to the inherently present crosslinking sites to stabilize the initially formed compartments. We here relied on RAFT-polymerization of a set of hydrophobic and hydrophilic monomers, reaching a sufficiently high molecular weight (> 30 kDa), coupled to the desired amphiphilic properties. The monomers, the chain transfer agent (CTA), and the crosslinking labels were synthesized according to literature with small adaptions (see Supporting Information).[14] The amphiphilic azide containing precursor polymer was synthesized by RAFT copolymerization of poly(ethylene glycol)$_n$ methacrylate (M_n (PEG) = 198 Da, n = 4.5, 85 mol%) and 3-azidopropyl methacrylate (15 mol%) in DMF using cyanoisopropyl dithiobenzoate (CPDB) as CTA and azobisisobutyronitrile (AIBN) as initiator. The CTA end group of the resulting polymer was removed using an excess of AIBN. Subsequently the polymer was purified by dialysis in THF (10 kDa cutoff) to obtain poly[(poly(ethylene glycol) methacrylate)-*co*-(3-azidopropyl methacrylate)] (PEAMA, M_n = 34.6 kDa, PDI = 1.4, DP = 129). The reached degree of polymerization of 129 and an azide content of 15 mol% allows an average of 19-20 crosslinking sites and thus 9-10 bivalent crosslinkers per collapsed polymer, prospectively embedding up to this number of label molecules, dependent on the ratio of the labeled crosslinker.

Single-chain collapse was accomplished in water and THF by CuAAC of pendant azide groups along the polymer chain together with external bis-alkynes as crosslinkers. This allows a fast and complete reaction of the crosslinkers in both reaction media, coupled to a complete removal of the Cu-salts after crosslinking.[15] Both, the precursor polymer and the crosslinker were dissolved in THF and added slowly either to a vigorously stirred aqueous solution containing $CuSO_4$, sodium ascorbate (NaAsc), and *N*,*N*,*N*′,*N*″,*N*″-pentamethyldiethylenetriamine (PMDTA) to achieve SCNPs with a compartmented core–shell structure; or to a vigorously stirred THF solution containing CuBr and 2,2'-bipyridine, to achieve SCNPs with a differently compartmented structure. The polymer-crosslinker solution was added via a syringe pump (10 mgmL^{-1}, 20 mL, 1 mLh^{-1}) ensuring low concentrations of reactive groups during the whole reaction time to prevent interchain crosslinking. As crosslinkers octadiyne (A), and the alkyne functionalized derivates of 2,2,6,6-tetramethylpiperidinyloxyl (TEMPO, B) or aza-BODIPY (C) were used as depicted in **Scheme 1**. To further achieve different label densities in the resulting SCNPs, different molar mixtures of octadiyne with aza-BODIPY or TEMPO were used during the collapse reaction, either with the pure crosslinker, or mixtures with 50 mol% octadiyne/50 mol% label, and with 75 mol% octadiyne/25 mol% label (see **Table 1**). The samples are named as SCNP$_{[\text{collapse medium}]}A_{[\text{mol\% octadiyne}]}B/C_{[\text{mol\% TEMPO or aza-BODIPY}]}$. Intense purification was done by extraction, column chromatography, and dialysis with different solvents (10 kDa cutoff, see Supporting Information for further details) to remove potentially unreacted label and residues of the copper catalysts. Complete reaction of all azides on the polymer side chains was followed by attenuated total reflection infrared (ATR-IR) spectroscopy, demonstrating the complete removal of the azide band at 2100 cm^{-1} under all reaction conditions as can be seen in Figure S1 (Supporting Information).

2.2. Single-Chain Nanoparticle Characterization

Diffusion-ordered NMR spectroscopy (DOSY-NMR) in D_2O, dynamic light scattering (DLS) in water, and size exclusion chromatography (SEC) in THF independently proved the formation of single-chain nanoparticles by showing reductions of the hydrodynamic diameters D_h for all SCNPs after the collapse reaction, compared to the precursor polymer PEAMA (see Table 1, **Figure 1**b, and Figures S2 and S4, Supporting Information). DLS measurements of aza-BODIPY labeled SCNPs were not possible due to absorption of the laser of the instrument (see Supporting Information). DOSY-NMR experiments showed size reductions of 4-53% for all SCNPs compared to the precursor polymer PEAMA as seen in Figure 1b. For the initial PEAMA a

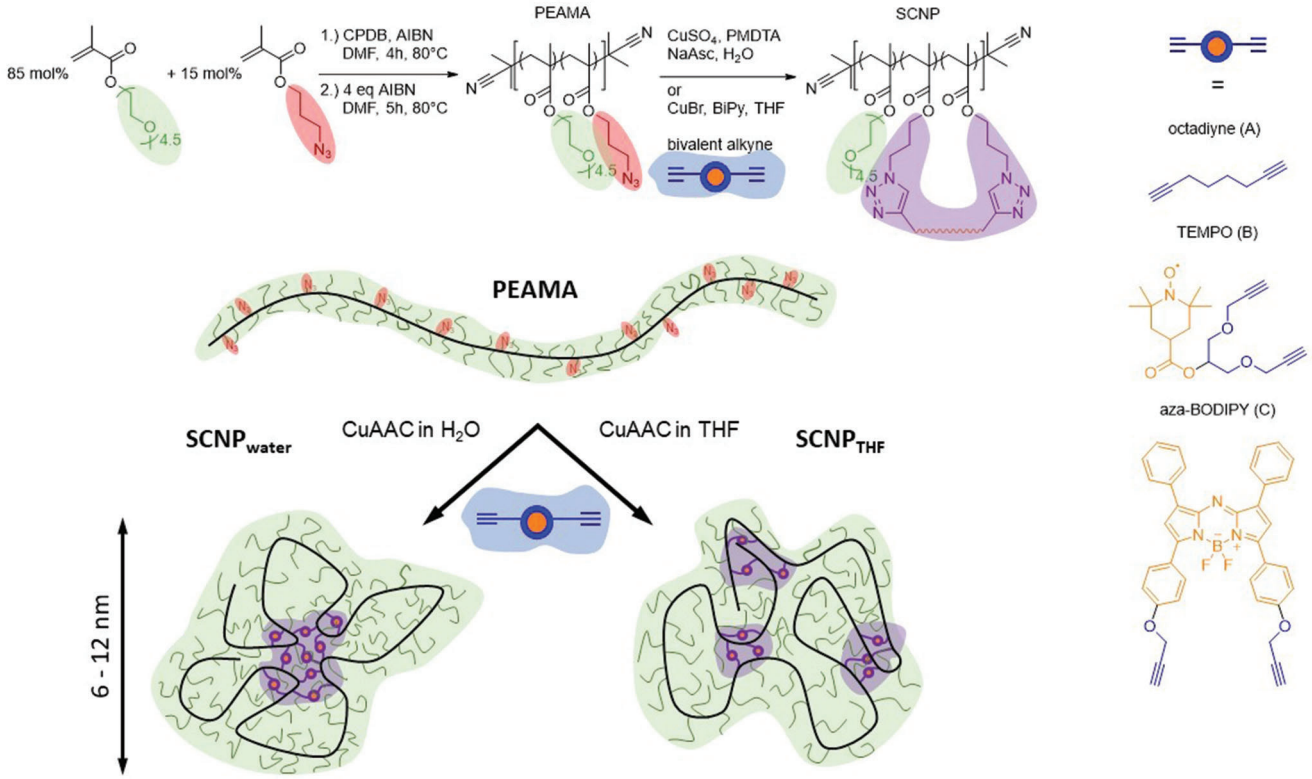

Scheme 1. RAFT polymerization of the precursor polymer PEAMA followed by single-chain collapse into labeled and unlabeled SCNPs in different reaction media and with different crosslinkers. All reaction conditions yielded SCNPs with hydrodynamic diameters of 6-12 nm. Collapse in different media resulted in the formation of different nanocompartments with the polar PEG chains (green) in the shell (green) and the non-polar crosslinking groups (azide—red, alkyne—blue, reacted crosslinkers—violet, labels—orange) in the compartmented crosslinked cores (violet).

Table 1. Data of the synthesized SCNPs and their precursor polymer PEAMA: label type, number of label molecules per SCNP, hydrodynamic diameter D_h as measured by DLS and DOSY-NMR, cloud point temperatures T_{cp} as measured by turbidimetry, and the average height in AFM topographies of the precursor polymer PEAMA and the resulting SCNPs.

Sample name	Label	Labels per particle[a)]	$D_{h,\,DLS}$[b,c)] [nm]	$D_{h,\,DOSY}$[d)] [nm]	T_{cp}[e)] [°C]	AFM height [nm]
PEAMA	–	–	10.4 ± 1.8	12.6 ± 0.11	57.9	21.5 ± 1.7[f)]
$SCNP_{water}A_{100}$	–	0	7.4 ± 1.3	7.8 ± 0.05	65.2	6.3 ± 0.5
$SCNP_{THF}A_{100}$	–	0	7.2 ± 1.1	5.8 ± 0.03	66.2	4.2 ± 0.5
$SCNP_{water}B_{100}$	TEMPO	9–10	8.9 ± 1.7	7.7 ± 0.13	61.2	5.8 ± 0.4
$SCNP_{THF}B_{100}$	TEMPO	9–10	8.2 ± 1.5	6.3 ± 0.01	62.9	1.7 ± 0.7
$SCNP_{water}A_{50}B_{50}$	TEMPO	4–5	9.1 ± 0.9	10.1 ± 0.06	60.7	8.6 ± 0.9
$SCNP_{THF}A_{50}B_{50}$	TEMPO	4–5	9.4 ± 1.1	11.3 ± 0.05	65.5	1.3 ± 0.1
$SCNP_{water}A_{75}B_{25}$	TEMPO	2–3	8.6 ± 1.5	11.6 ± 0.02	59.5	5.8 ± 0.4
$SCNP_{THF}A_{75}B_{25}$	TEMPO	2–3	9.8 ± 1.5	12.1 ± 0.15	71.5	3.5 ± 0.5
$SCNP_{water}C_{100}$	aza-BODIPY	9–10	–	9.7 ± 0.17	59.5	5.4 ± 0.1
$SCNP_{THF}C_{100}$	aza-BODIPY	9–10	–	10.6 ± 0.10	67.5	5.5 ± 0.2
$SCNP_{water}A_{50}C_{50}$	aza-BODIPY	4–5	–	9.4 ± 0.03	57.4	3.6 ± 0.4
$SCNP_{THF}A_{50}C_{50}$	aza-BODIPY	4–5	–	7.4 ± 0.05	70.4	4.9 ± 0.1
$SCNP_{water}A_{75}C_{25}$	aza-BODIPY	2–3	–	9.4 ± 0.04	62.5	3.2 ± 0.4
$SCNP_{THF}A_{75}C_{25}$	aza-BODIPY	2–3	–	7.2 ± 0.12	67.8	3.2 ± 0.1

[a)] Calculated from the initial mol% of azide monomer during polymerization, the Mn of the precursor polymer PEAMA, and the mol% of labeled crosslinker during the collapse reaction. [b)] Measured by DLS in H_2O at 1 mgmL^{-1}. [c)] DLS measurements for aza-BODIPY labeled SCNPs were not possible due to absorption of the irradiation wavelength of the scattering laser. [d)] Measured by DOSY-NMR in D2O at 1 mg mL^{-1}, calculated using the Stokes–Einstein equation ($D_h = (k_B \bullet T)/(3 \bullet \pi \bullet \eta \bullet D)$ with the diffusion coefficient D, η_{D2O} = 1.25 mPa s). [e)] Cloud point temperature measured by turbidimetry at concentrations of 1 mgmL^{-1}, $T_{cp} = T$ at 50% transmittance. [f)] Larger size for PEAMA caused by agglomeration of multiple polymer chains, no single chains were detectable.

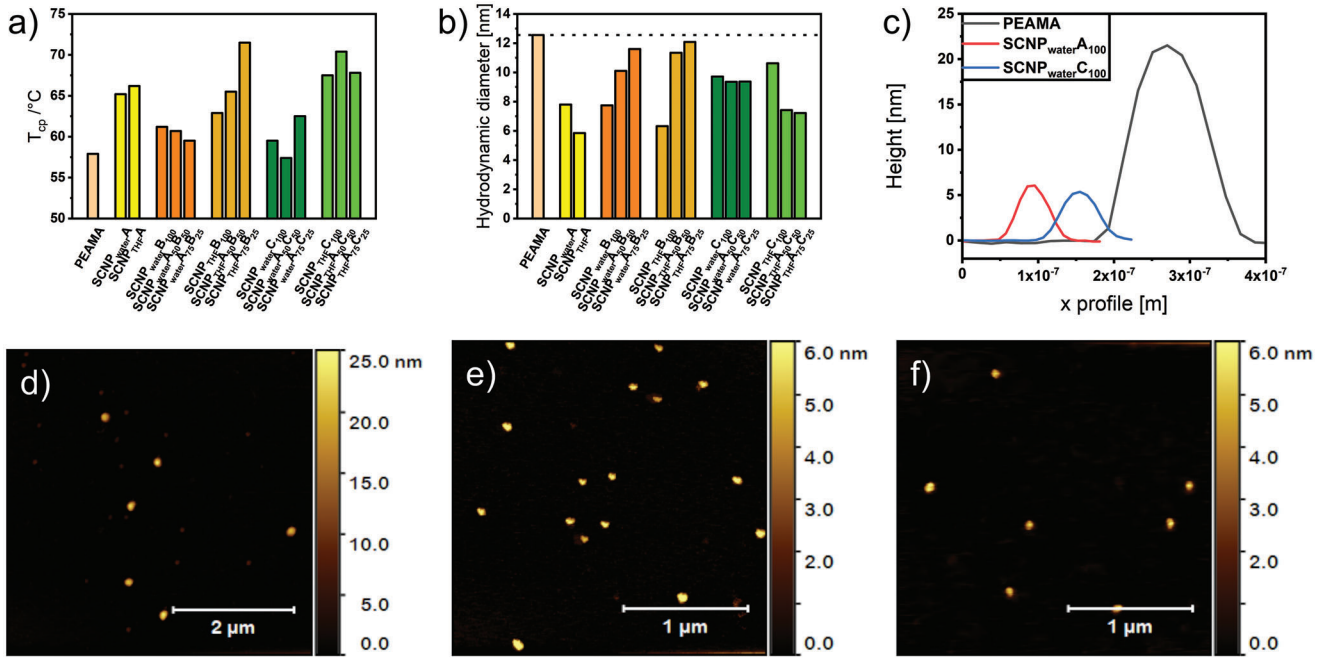

Figure 1. a) Cloud point temperatures T_{cp} of the precursor polymer PEAMA and the SCNPs. Complete turbidimetry measurements are shown in Figure S5, Supporting Information. b) Hydrodynamic diameter of PEAMA and the SCNPs as determined by DOSY-NMR. c) Average profiles of the precursor polymer PEAMA, $SCNP_{water}A_{100}$, and $SCNP_{water}C_{100}$, as extracted from AFM topographies. d–f) AFM topographies of PEAMA, $SCNP_{water}A_{100}$, and $SCNP_{water}C_{100}$, respectively. AFM topographies of all SCNPs are shown in Figure S6, Supporting Information.

hydrodynamic diameter of 12.6 nm was measured. The strongest size reduction was found for $SCNP_{THF}A_{100}$ with a hydrodynamic diameter of 5.8 nm. DOSY-NMR also revealed that the size reduction is dependent on the crosslinker mixture. Adding B and octadiyne as crosslinkers during the collapse is leading to an increased hydrodynamic diameter from 7.7 nm for $SCNP_{water}B_{100}$ and 6.3 nm for $SCNP_{THF}B_{100}$ to 11.6 nm for $SCNP_{water}A_{75}B_{25}$ and 12.1 nm for $SCNP_{THF}A_{75}B_{25}$, respectively. We attribute this effect either to long range crosslink reactions being less effective for the crosslinker mixtures, or to a less effective pre-collapsing behavior when octadiyne and B are mixed during the collapse.[10] This effect is not present for the aza-BODIPY dye C showing that the long-range crosslink and pre-collapsing behavior of C is less effected when mixed with octadiyne.

In contrast to SEC measurements in THF, SEC measurements in water show an exact opposite behavior of the peak shifts for the labeled SCNPs as seen in Figure S3 (Supporting Information). As reported earlier,[12a] this behavior is caused by changes of the polarity of the polymer in response to the surrounding solvent. As after single-chain collapse the nonpolar crosslinking groups are in reduced contact with the aqueous solvation shell, the now increased polarity of the particle shell leads to a partially enthalpic, and therefore not only size but also polarity driven separation on the aqueous SEC column, an effect already described by Barner-Kowollik et al.[16] The formation of those compartments of different polarity is also evident in the LCST-behavior of the precursor polymer and the therefrom derived SCNPs in Figure 1a and Figure S5 (Supporting Information): collapsing the polymer into SCNPs always leads to higher cloud point temperatures, caused by the formation of hydrophobic compartments within the SCNPs, with the crosslinking groups located in these compartments, expectedly surrounded by the hydrophilic PEG side chains, thus increasing the SCNP's solubility in water. A second effect in the T_{cp} measurements is the difference caused by the choice of the collapse medium. SCNPs collapsed in THF always tend to display higher T_{cp} values than those collapsed in water. This effect can be attributed to the formation of more open structures when the collapse is performed in THF, in turn increasing the SCNP's solubility and thus its T_{cp}. In contrast, single-chain collapse in water leads to the formation of denser structures with lower water permeability. Together with the results from SEC, this is a first indication of the formation of different compartments inside the SCNPs depending on the surrounding medium during single-chain collapse.

As electron microscopy (TEM) did not yield interpretable pictures, we further proved the formation of distinct single-chain nanoparticles by atomic force microscopy (AFM) topographies as seen in Figure 1c-f and Figure S6 (Supporting Information). The average height of the precursor polymer PEAMA on the mica surface was found to be 21.5 nm (Figure 1d) showing agglomerations of multiple polymer chains on the surface, with single polymer chains not detectable. The AFM topography images of $SCNP_{water}A_{100}$ and $SCNP_{water}C_{100}$ in Figure 1e,f show single particles on the mica surface with average heights of 6.3 and 5.4 nm, respectively. Although all average heights of the SCNPs found by AFM (see Figure S6, Supporting Information for all topographies) are smaller than the hydrodynamic diameters measured by DLS and DOSY-NMR, the values are fitting well since SCNPs tend to lose their spherical shape on the mica surface and therefor display smaller sizes.[17] Additionally, AFM measures the heights

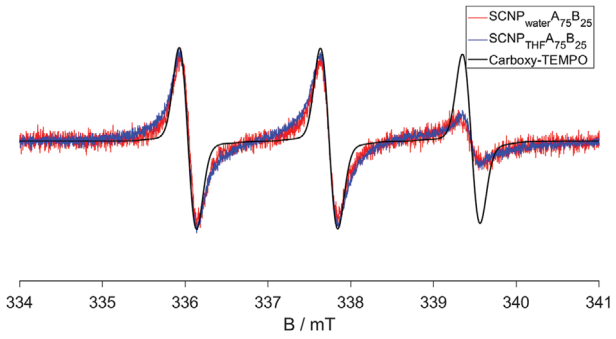

Figure 2. EPR-spectra of $SCNP_{water}A_{75}B_{25}$ and $SCNP_{THF}A_{75}B_{25}$ measured in water at 20 °C with a concentration of 10 mgmL^{-1} in water, and of carboxy-TEMPO measured in water at 20 °C with a concentration of 1 mM in water. The spectra were normalized to the center peak.

of the particles without their solvation shell leading to apparently smaller values.

2.3. Internal Structure Analysis of Differently Collapsed SCNPs by EPR Spectroscopy

Labeling SCNPs with TEMPO (B) enabled to probe location, distribution, and movement of the labeled crosslinkers inside the SCNPs via electron-paramagnetic-resonance (EPR) spectroscopy. When compared to the EPR spectra of the non-bound nitroxide radical, strong changes in the spectra of the nitroxide labeled SCNPs prove the formation of differently compartmented structures, dependent on the collapse media and the crosslinker mixtures that were used as shown in **Figure 2**. Simulations of the measured spectra (see Figures S7 and S8, and Table S1, Supporting Information) revealed the presence of up to three label species per SCNP, additionally proving the formation of compartments. For all labeled SCNPs Heisenberg coupling was found with exchange coupling constants of 2.5–3.0 MHz, with higher values for those SCNPs synthesized in water (see Table S1, Supporting Information): an important effect, as Heisenberg coupling only occurs, when two or more labels get closer than 1 nm, thus proving that the labels are concentrated into specific compartments rather than being homogeneously distributed along the SCNP.[12] The τ values in species 1 (see Table S1, Supporting Information), which represent the rotational mobility of the TEMPO labels, were measured to be higher for those SCNPs that were synthesized in water, hence showing a stronger reduction in mobility for those labels. As proposed from the results from the T_{cp} measurements, this is a further proof of the formation of denser compartments for these SCNPs and therefore of less dense compartments for those SCNPs synthesized in THF. Simulations of the spectrum of $SCNP_{water}B_{100}$ revealed the presence of a third species without Heisenberg coupling. This indicates a position of these label molecules outside the compartments with a distance of more than 1 nm from other labels. In addition, lower τ values indicate a much faster movement. Hence, this label species is located on the outer shell of the particles where its movement is less strong hindered. This proves that a collapse in water without a second, unlabeled crosslinker results in a reduced compartmentation and a less pronounced effective core–shell structure.

2.4. Influence of Different Compartmentations on Photophysical Properties of Fluorescent SCNPs

The effect of the compartmentation of the SCNPs on the optical and thermomechanical properties of the dye aza-BODIPY (**C**) as crosslinker is important for their envisaged application as contrast agent in fluorescence and PA imaging, as high extinction coefficients, high fluorescence quantum yields, and long fluorescence lifetimes are advantageous for the desired pump–probe excitation.[18] The absorption and fluorescence spectra of non-bound aza-BODIPY in water are shown in Figures S9 and S10 (Supporting Information). Since the dye itself is not soluble in water, it was kept in aqueous solution with the surfactant Kolliphor EL (see Supporting Information). The absorption spectrum shows a maximum at 695 nm with Lambert–Beer behavior over the entire concentration range (see Figure S9b, Supporting Information). The fluorescence spectra in Figure S10 (Supporting Information) with a maximum at 720 nm lose their linear behavior at concentrations higher than 8×10^{-6} M. The effects of high concentrations on the fluorescence intensity and the wavelength maximum are shown in Figure S10b,c (Supporting Information).

Covalently binding the aza-BODIPY dye to the nanoparticles significantly changes its optical behavior as seen in **Figure 3**a,b. In the absorption spectra of water collapsed SCNPs in Figure 3a the shoulder at 647 nm shows an increased intensity compared to the non-bound dye, independently from the aza-BODIPY load inside the particle. Additionally there is a new absorption band for $SCNP_{water}A_{50}C_{50}$ at 765 nm. The absorption spectra of the THF collapsed SCNPs in Figure 3b show a markedly different behavior with an absorption band at 647 nm that increases with increasing aza-BODIPY content per particle, caused by the formation of different types of compartments inside the SCNPs depending on the collapse medium and the ratio between aza-BODIPY and octadiyne during the crosslink reaction.

The internal structure of the SCNPs and the dye content has a significant effect on the fluorescence intensity and thus their usefulness for pump–probe excitation. When collapsed in THF, the incorporation of the aza-BODIPY molecules to the SCNP leads to a decreased fluorescence intensity (see Figure 3b) which is reduced further with increasing aza-BODIPY load inside the particle by fluorescence quenching indicative of a rather polar environment of the dye molecules with direct contact to water for this type of SCNPs. By contrast, water-collapsed SCNPs form a core–shell structure where the aza-BODIPY molecules are located in the non-polar core of the particle due to their hydrophobicity. The fluorescence spectra of the co-crosslinked SCNPs that were collapsed in water support this hypothesis by showing a significant increase in intensity. Additionally, $SCNP_{water}A_{75}C_{25}$ shows a fluorescence intensity that is only 25% lower than that of $SCNP_{water}A_{50}C_{50}$ even though the dye concentration is 50% lower indicating a more effective formation of the non-polar core. When aza-BODIPY is solely used as crosslinker during the collapse reaction, the formation of a core–shell structure is less effective, inline with EPR measurements. This increases the polarity of the surrounding medium of the individual dye molecules in the SCNP, yielding lower fluorescence intensities (see **Scheme 2**).

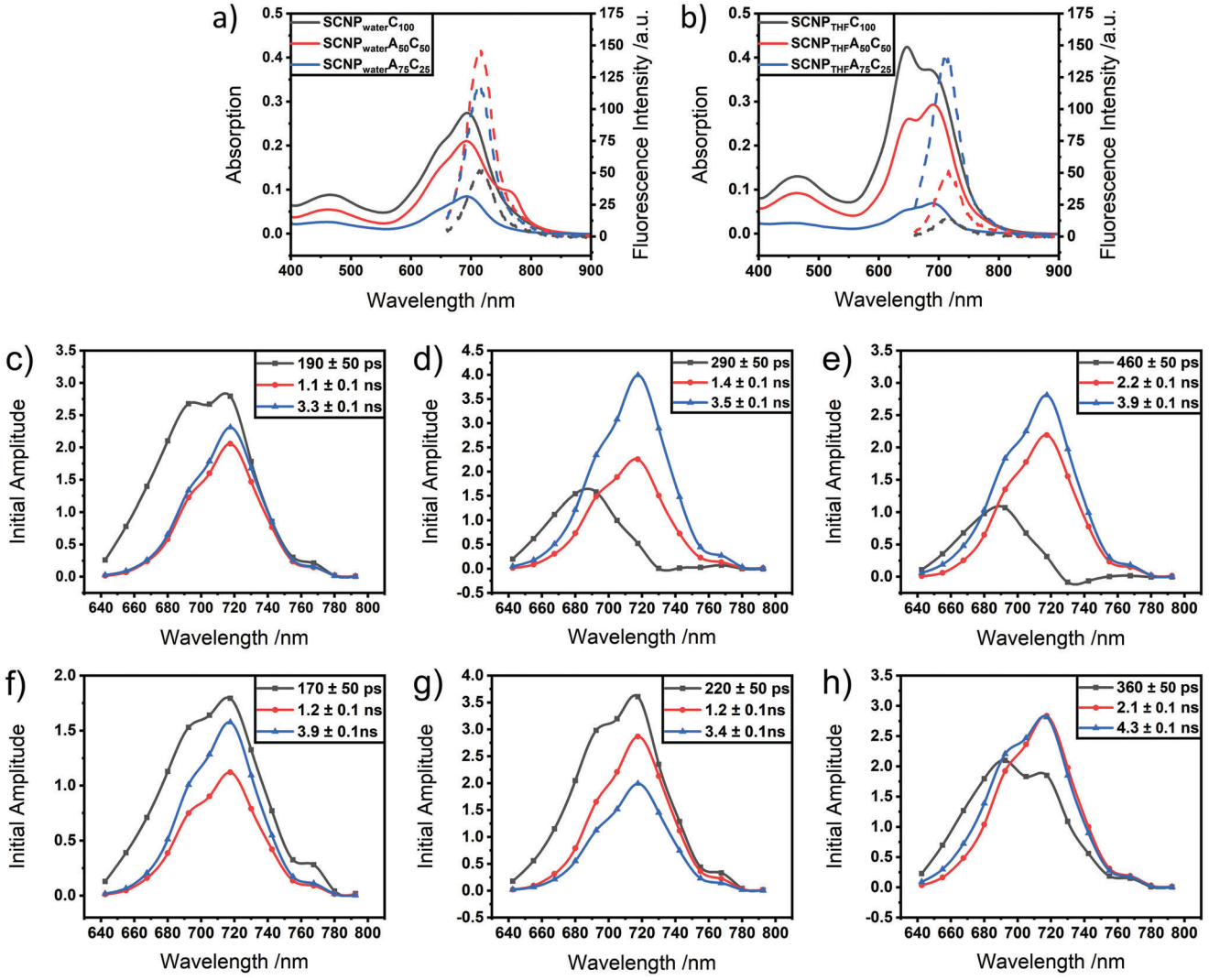

Figure 3. Absorption (solid line) and fluorescence (dashed line) spectra of a) water-collapsed and b) THF-collapsed aza-BODIPY labeled SCNPs at concentrations of 0.1 mgmL^{-1} in water. λ_{ex} = 650 nm, slit = 5 nm, $V_{detector}$ = 600 V. Decay associated spectra of c) SCNP$_{water}$C$_{100}$, d) SCNP$_{water}$A$_{50}$C$_{50}$, e) SCNP$_{water}$A$_{75}$C$_{25}$, f) SCNP$_{THF}$C$_{100}$, g) SCNP$_{THF}$A$_{50}$C$_{50}$, h) SCNP$_{THF}$A$_{75}$C$_{25}$ at concentrations of 0.1 mgmL^{-1} in water.

To further check for the exact location of the fluorescent labels inside the SCNP's compartments and how this influences the optical properties of aza-BODIPY including its fluorescence lifetime, decay-associated spectra (DAS)[19] were measured. DAS of the free dye are shown in Figure S11 (Supporting Information). In aqueous solution, aza-BODIPY exhibits a fast decay of 260 ps, as a polar solvation, especially with water, quenches the first excited singlet state.[12a] However, the surfactant Kolliphor EL reduces the environments polarity resulting in additional slow decay components (red and blue curves in Figure S11, Supporting Information, respectively).

The decay associated spectra for aza-BODIPY labeled SCNPs in Figure 3c–h also represent three fluorescence components. While all THF-collapsed SCNPs and SCNP$_{water}$C$_{100}$ show a dominant short-lived component, two water-synthesized SCNPs, i.e., SCNP$_{water}$A$_{50}$C$_{50}$ and SCNP$_{water}$A$_{75}$C$_{25}$, show dominant long-lived lifetimes ranging from 2.1 to 4.3 ns (Figure 3d,e). In addition, the lifetime of the fast component is gradually increasing as the number of aza-BODIPY molecules per SCNP is reduced. For SCNP$_{water}$C$_{100}$, for example, the lifetime of 190 ns indicates that that a large fraction of the aza-BODIPY molecules is located in a polar environment. This situation is different for SCNP$_{water}$A$_{75}$C$_{25}$ where the time constant increases to 460 ps. This would suggest that here the dye molecules are encapsulated in the core of the particle and therefore shielded from the quenching effects of water. For SCNPs collapsed in THF, the fraction of aza-BODIPY in a polar environment is proportional to the aza-BODIPY content.

In the water-collapsed and co-crosslinked SCNPs, an additional heterogeneity in the fast-lived component is observed as evidenced by a maximum at 690 nm and a minimum (negative amplitude) at 730 nm (Figure 3d,e, black curves). Direct contact between individual dye molecules is leading to the formation of excitonic couples,[12a] inline with the Heisenberg exchange found in the EPR measurements, an important effect since it increases fluorescence lifetimes and intensities.

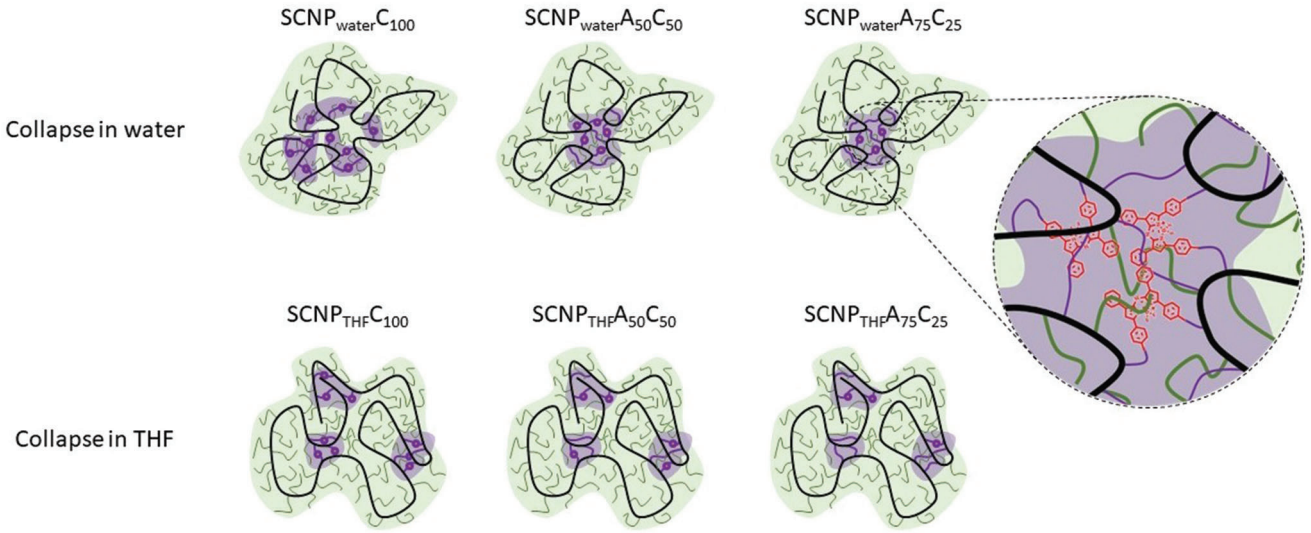

Scheme 2. Schematic interpretation of the spatial distribution of aza-BODIPY inside the nanoparticles depending on the collapse medium and the amount of label crosslinker. Collapse in different media resulted in the formation of different nanocompartments with the polar PEG chains (green) in the shell (green) and the non-polar crosslinking groups (violet, aza-BODIPY—red) in the compartmented crosslinked cores (violet).

The overall picture of the compartments formed by collapse and crosslinking in different media is schematically shown in Scheme 2. Thus collapse in either water or in THF resulted in the formation of different nanosized compartments inside the SCNPs, with the polar PEG chains (green) in the shell (green) and the non-polar crosslinking groups (violet, aza-BODIPY—red) in the compartmented crosslinked cores (violet). It must be noted that—as expected—collapse in water leads to the formation of core–shell structured SCNPs, although there is an influence of the molar ratio of the labeled crosslinker on the final structure. Collapse in THF leads to a more open structure, where the dyes are located in several smaller compartments inside a looser and rather hydrophilic core.

2.5. Application of Compartmented Fluorescent SCNPs as Contrast Agents for Photoacoustic Measurements

The compartmented structure and specific composition of the SCNPs also resulted in marked differences in the amplitude and time-course of photoacoustic (PA) signals. PA waves are generated by the absorption of short excitation pulses (several ns duration) by absorbing chromophores. The optical energy is converted to heat and initial pressure which relaxes by emitting a broadband ultrasound wave. Using an ultrasound transducer, time-resolved signals are acquired. Under conditions of thermal and stress confinement and for simple geometries, such as cuvettes, the time-course of the signals can be assumed to represent the axial distribution of the absorbed optical energy along the excitation beam. PA signals generated using pump–probe excitation, i.e., using excitation pulses at different wavelengths and time delays, allow information on the dynamics of absorption and relaxation from excited states in fluorophores to be obtained.[18,20] Here, we apply this method to investigate the correlation between the structure and composition of the SCNPs, their optical properties as represented by the decay associated spectra, and PA data.

Details of the experimental setup and the methods are given in the Supporting Information. PA signals were measured at room temperature in aqueous SCNP solutions with a concentration of 1 mgmL^{-1} using pump and probe wavelengths that coincided with the wavelengths of peak absorption and fluorescence ($\lambda_{probe} = 690$ nm, $\lambda_{probe} = 730$ nm). **Figure 4**a–c shows time-resolved PA signals acquired using pump–probe time delays of 0, 5, and 10 ns. The signal amplitudes are normalized with respect to SCNP absorption at the pump and probe wavelengths. Each graph shows two sets of PA signals measured in solutions of water-collapsed (solid lines) or THF-collapsed (dashed lines) SCNPs with identical dye load. Since the time-course of the PA signals corresponds to the absorbed energy distribution along the axis of the excitation beam, qualitative comparisons of the absorption and relaxation dynamics between the different SCNPs can be made. In Figure 4a–c, the boundaries of the sample volume within the cuvette are indicated by dashed lines. The early arriving signal around 0.6–1.0 µs corresponds to the PA wave from the back of the cuvette, while the signal at 4.4 µs originates from the illuminated side. Marked differences in the shape of the signals measured in water- and THF-collapsed SCNPs are observed. In Figure 4a,b, the signal amplitude generated adjacent to the illuminated window (between 3.0 and 4.4 µs) is lower in water-collapsed SCNPS than in those collapsed in THF. This difference is likely due to the more dominant slow decay component in water-collapsed SCNPs (see Figure 3), which results in ground state depopulation in regions of high fluence. This, in turn, reduces the absorbed energy density, and hence PA signal amplitude generated in the sample volume adjacent to the illuminated window. THF-collapsed particles, by comparison, exhibit predominately fast relaxations (see Figure 3), which prevents ground state depopulation and results in a larger PA signal amplitude near the source. The time-course of these signals also approaches the typical exponential shape expected of absorbers with short lifetimes. Although the signals acquired in SCNPs with minimal dye load, i.e., SCNP$_{water}$A$_{75}$C$_{25}$ and SCNP$_{THF}$A$_{75}$C$_{25}$, show

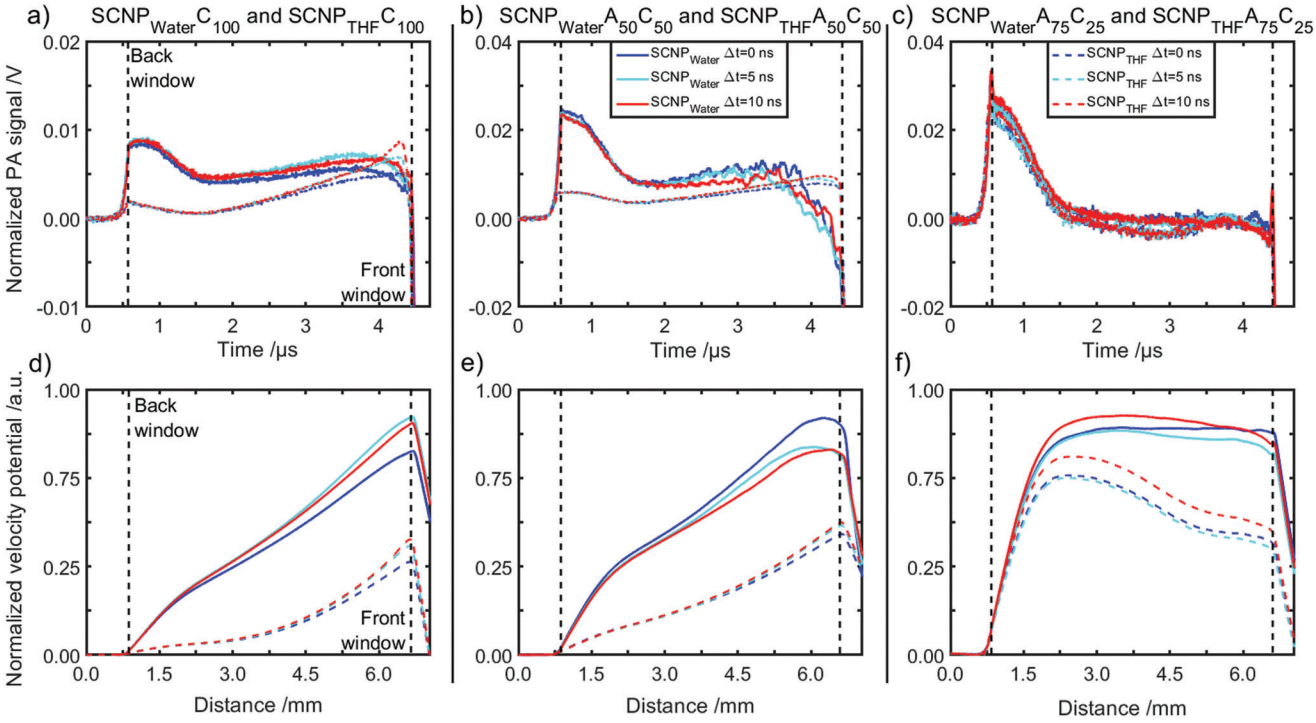

Figure 4. a–c) Absorption normalized PA pump–probe signals measured in aza-BODIPY labeled SCNP solutions and d–f) the corresponding velocity potential at time delays of 0 ns (blue), 5 ns (cyan), and 10 ns (red). The concentration of SCNP was 1 mgmL^{-1}, and the pump and probe fluences were Φ_{pump} = 8.0 mJcm^{-2} and Φ_{probe} = 13.4 mJcm^{-2}. The solid lines show the PA signals and velocity potentials measured in water-collapsed SCNPs, while the dashed lines show the data acquired in THF-collapsed SCNPs. The vertical dashed lines indicate the location of the cuvette windows.

similar features (Figure 4c), they are not easily discerned due to low signal-to-noise ratios (SNR).

To improve SNR and to obtain a qualitative measure of the total initial pressure that was generated in the SCNP solutions, the velocity potential was calculated by time-integrating the PA signals. The velocity potential is shown in Figure 4d–f as a function of depth assuming the speed of sound in water. The peak values of the velocity potentials suggest that the total initial pressure is larger in water-collapsed SCNPs compared those collapsed in THF. This may be explained by differences in the Grüneisen parameter that are a consequence of the compartmentation in the different SCNPs. In THF collapsed particles, the dye molecules are distributed randomly across the particles and are therefore likely to be quenched by water. In water-collapsed SCNPs, by contrast, the dye molecules accumulate at the core surrounded by the polymer. Since the polymer is expected to exhibit a larger Grüneisen parameter than water, the PA signal and the velocity potential is larger in water-collapsed SCNPs. The pump–probe time delay was also found to modulate the PA signal in ways that appear to be dependent upon the particle structure and composition. In most SCNPs, the change in the PA signal near the cuvette was modest and increased with time delay. Only the water-collapsed particles with low dye load, i.e., SCNP$_{water}$A$_{50}$C$_{50}$ and SCNP$_{water}$A$_{75}$C$_{25}$, exhibited the behavior expected of fluorophores,[18] i.e., an increase in signal amplitude and velocity potential was observed for a time delay of 0 ns compared to 5 ns and 10 ns (Figure 4b,c,e,f). This observation can again be explained by the dominant long-lived excited states of these particles (Figure 3) as compared to the other SCNPs. Since the pump-probe induced change in signal amplitude is the contrast mechanism in molecular PA imaging applications, SCNP$_{water}$A$_{50}$C$_{50}$ would appear to possess the most advantageous properties.

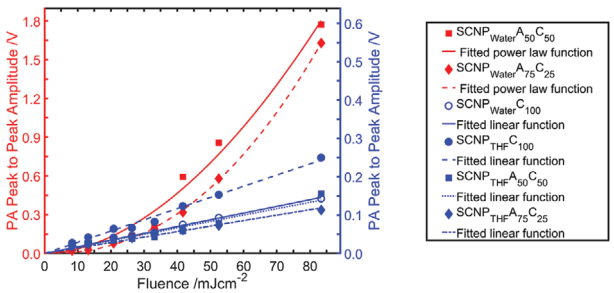

Figure 5. The absorption normalized PA signal amplitude measured in aza-BODIPY labeled SCNPs as a function of the incident fluence. A linear dependence was observed in THF-collapsed particles and water-collapsed particles with a high dye load, i.e., SCNP$_{water}$C$_{100}$, as illustrated by linear regressions (blue symbols and lines). Water-collapsed SCNPs (SCNP$_{water}$A$_{50}$C$_{50}$, SCNP$_{water}$A$_{75}$C$_{25}$) with a dye load of up to 50% exhibit a nonlinear fluence dependence (red symbols) which was found to agree with a quadratic fit function (red lines). The SCNP concentrations were 1 mg mL^{-1} in water.

Figure 5 shows the fluence dependence of the PA signal amplitude measured in the SCNP solutions for a pump–probe time delay of 0 ns. The fluence was set using ND filters and ranged from 8.5 to 85.3 mJcm^{-2}. SCNP$_{water}$C$_{100}$ and the SCNPs collapsed in THF show a linear increase in signal with modest

signal amplitudes. By contrast, two of the SCNPs collapsed in water ($SCNP_{water}A_{50}C_{50}$, $SCNP_{water}A_{75}C_{25}$) show a strong nonlinear fluence dependence with signal amplitudes up to two orders of magnitude greater than that of equivalent THF-collapsed SCNPs. The origin of this nonlinearity is unclear. Possible explanations may include a heat-induced change in the thermomechanical properties, such as the Grüneisen parameter, due to the strong spatial confinement of the dye molecules, or interactions between molecules in an excited state. An immediate benefit of the nonlinear fluence dependence arises in in vivo applications of the particles where it can be exploited as a contrast mechanism.[21]

3. Conclusion

In summary, we were able to generate dye-loaded, compartmented single-chain nanoparticles by collapse in reaction media of different polarity. Using differently labeled crosslinkers we could analyze the influence of the crosslinker and the collapse medium on the nanosized compartmentation of the individual particles and how these can be used to tune the optical properties for applications in fluorescence tomography and photoacoustic measurements. Collapsing the PEGMA copolymer with azide side chains using copper catalyzed azide-alkyne click reactions in water resulted in the formation of core–shell structured particles with the hydrophobic groups in the core and the hydrophilic PEG side chains in the shell. Collapse in THF resulted in looser compartmented particles in which the hydrophobic groups were located in multiple smaller compartments distributed over the whole particle. The formation of those compartments was followed by using water based SEC and T_{cp} measurements individually showing changes in the water solubility of the SCNPs and therefore their polarity. One proof of the formation of the compartmented structures was accomplished by EPR spectroscopy after introducing a TEMPO label as crosslinker. Simulations of the measured spectra revealed large Heisenberg exchange coupling with high τ values for all SCNPs, demonstrating close contact for the labels with distances in the subnanometer range. Collapsing the TEMPO labeled SCNPs in water resulted in higher τ values, revealing a denser encapsulation of the labels at the core. Labeling the SCNPs with the fluorescent dye aza-BODIPY as a crosslinker enabled an independent validation of these compartmented structures using optical methods. Depending on the degree of compartmentation, SCNPs showed differences in the absorption and fluorescence spectra. New absorption bands and strong differences in fluorescence intensities were observed depending on the collapse medium and dye load. In the core–shell structured particles, excitonic couples and non-polar environments for the dye molecules were generated, yielding increased fluorescence lifetimes and intensities. The compartments are advantageous for PA measurements, which showed that water-collapsed SCNPs with comparatively low dye loads possess advantageous properties compared to THF-collapsed particles. Most importantly increased signal generation efficiency, susceptibility to contrast mechanisms based on pump–probe excitation, and a non-linear fluence dependence of the signal amplitude were observed, which can be exploited as a contrast mechanism.

The concept described in this paper therefore paves the way toward precise engineering of nanosized contrast agents for imaging technologies, where the tuning of photophysical and thermomechanical properties is required. Applications in biomedical fluorescence and PA imaging are particularly attractive, as SCNPs may offer new contrast mechanisms, which could include the multiplexed detection of contrast agents based on differences in the lifetime and nonlinearity, and the use of SCNPs as biosensors.

4. Experimental Section

Detailed information on the materials, all methods, and syntheses are given in the Supporting Information.

Supporting Information

Supporting Information is available from the Wiley Online Library or from the author.

Acknowledgements

The authors thank the DFG-Graduate College GRK 2670 (German research foundation-project D43649874, TP B2, RTG 2670) for financial support (WHB, JFT). J.L. acknowledges funding by the DFG via project grant LA3273/7-1. D.H. acknowledges funding by TP A2 (DH) in the GRK 2670.
Open Access funding enabled and organized by Projekt DEAL.

Conflict of Interest

The authors declare no conflict of interest.

Data Availability Statement

The data that support the findings of this study are available in the supplementary material of this article.

Keywords

decay-associated spectra, EPR spectroscopy, fluorescence spectroscopy, nanocompartments, photoacoustic imaging, single-chain nanoparticles

Received: July 13, 2022
Revised: August 5, 2022
Published online: August 27, 2022

[1] a) Y. Bai, X. Feng, H. Xing, Y. Xu, B. K. Kim, N. Baig, T. Zhou, A. A. Gewirth, Y. Lu, E. Oldfield, S. C. Zimmerman, *J. Am. Chem. Soc.* **2016**, *138*, 11077; b) Y. Liu, S. Pujals, P. J. M. Stals, T. Paulöhrl, S. I. Presolski, E. W. Meijer, L. Albertazzi, A. R. A. Palmans, *J. Am. Chem. Soc.* **2018**, *140*, 3423; c) H. Rothfuss, N. D. Knofel, P. W. Roesky, C. Barner-Kowollik, *J. Am. Chem. Soc.* **2018**, *140*, 5875; d) S. Garmendia, S. B. Lawrenson, M. C. Arno, R. K. O'reilly, D. Taton, A. P. Dove, *Macromol. Rapid Commun.* **2019**, *40*, 1900071; e) T. Terashima, T. Mes, T. F. A. De Greef, M. A. J. Gillissen, P. Besenius, A. R. A. Palmans, E. W. Meijer, *J. Am. Chem. Soc.* **2011**, *133*, 4742; f) A. Sanchez-Sanchez, A. Arbe, J. Kohlbrecher, J. Colmenero, J. A. Pomposo, *Macromol. Rapid Commun.* **2015**, *36*, 1592.

[2] X. Tian, R. Xue, F. Yang, L. Yin, S. Luan, H. Tang, *Biomacromolecules* **2021**, *22*, 4306.
[3] a) N. M. Hamelmann, J.-W. D. Paats, J. M. J. Paulusse, *ACS Macro Lett.* **2021**, *10*, 1443; b) L. Deng, L. Albertazzi, A. R. A. Palmans, *Biomacromolecules* **2021**, *23*, 326; c) A. P. P. Kroger, M. I. Komil, N. M. Hamelmann, A. Juan, M. H. Stenzel, J. M. J. Paulusse, *ACS Macro Lett.* **2019**, *8*, 95; d) A. P. P. Kroger, N. M. Hamelmann, A. Juan, S. Lindhoud, J. M. J. Paulusse, *ACS Appl. Mater. Interfaces* **2018**, *10*, 30946.
[4] S. Liu, J. Rong, R. Liu, J. S. Lindsey, *ACS Appl. Polym. Mater.* **2021**, *3*, 1767.
[5] a) R. Gracia, M. Marradi, U. Cossío, A. Benito, A. Pérez-San Vicente, V. Gómez-Vallejo, H.-J. Grande, J. Llop, I. Loinaz, *J. Mater. Chem. B* **2017**, *5*, 1143; b) Y. Koda, T. Terashima, M. Sawamoto, H. D. Maynard, *Polym. Chem.* **2015**, *6*, 240.
[6] J. T. Offenloch, J. Willenbacher, P. Tzvetkova, C. Heiler, H. Mutlu, C. Barner-Kowollik, *Chem. Commun.* **2017**, *53*, 775.
[7] a) J. Nam, S. Kwon, Y.-G. Yu, H.-B. Seo, J.-S. Lee, W. B. Lee, Y. Kim, M. Seo, *Macromolecules* **2021**, *54*, 8829; b) K. Watanabe, N. Kaizawa, B. J. Ree, T. Yamamoto, K. Tajima, T. Isono, T. Satoh, *Angew. Chem., Int. Ed.* **2021**, *60*, 18122; c) Y. M. S. Nomura, T. Ikeda, M. Seki, M. Kamachi, *Macromolecules* **1995**, *28*, 2874; d) J. Rubio-Cervilla, H. Frisch, C. Barner-Kowollik, J. A. Pomposo, *Macromol. Rapid Commun.* **2019**, *40*, 1800491.
[8] a) T. S. Fischer, D. Schulze-Sunninghausen, B. Luy, O. Altintas, C. Barner-Kowollik, *Angew. Chem., Int. Ed.* **2016**, *55*, 11276; b) T. Terashima, T. Sugita, K. Fukae, M. Sawamoto, *Macromolecules* **2014**, *47*, 589.
[9] a) E. Verde-Sesto, A. Arbe, A. J. Moreno, D. Cangialosi, A. Alegrã-A, J. Colmenero, J. A. Pomposo, *Mater. Horiz.* **2020**, *7*, 2292; b) K. Watanabe, R. Tanaka, K. Takada, M.-J. Kim, J.-S. Lee, K. Tajima, T. Isono, T. Satoh, *Polym. Chem.* **2016**, *7*, 4782.
[10] S. Liao, L. Wei, L. A. Abriata, F. Stellacci, *Macromolecules* **2021**, *54*, 11459.
[11] C. H. Liu, L. D. Dugas, J. I. Bowman, T. Chidanguro, R. F. Storey, Y. C. Simon, *Polym. Chem.* **2020**, *11*, 292.
[12] a) J. F. Hoffmann, A. H. Roos, F. J. Schmitt, D. Hinderberger, W. H. Binder, *Angew. Chem., Int. Ed.* **2021**, *60*, 7820; b) A. H. Roos, J. F. Hoffmann, W. H. Binder, D. Hinderberger, *Soft Matter* **2021**, *17*, 7032.
[13] J. Weber, P. C. Beard, S. E. Bohndiek, *Nat. Methods* **2016**, *13*, 639.
[14] a) M. Abellan-Flos, M. Tanc, C. T. Supuran, S. P. Vincent, *J. Enzyme Inhib. Med. Chem.* **2016**, *31*, 946; b) S. H. Thang, B. Y. K. Chong, R. T. A. Mayadunne, G. Moad, E. Rizzardo, *Tetrahedron Lett.* **1999**, *40*, 2435; c) B. S. Sumerlin, N. V. Tsarevsky, G. Louche, R. Y. Lee, K. Matyjaszewski, *Macromolecules* **2005**, *38*, 7540; d) J. Murtagh, D. O. Frimannsson, D. F. O'Shea, *Org. Lett.* **2009**, *11*, 5386; e) D. Wu, D. F. O'Shea, *Tetrahedron Lett.* **2017**, *58*, 4468.
[15] a) W. H. Binder, R. Sachsenhofer, *Macromol. Rapid Commun.* **2007**, *28*, 15; b) W. H. Binder, R. Sachsenhofer, *Macromol. Rapid Commun.* **2008**, *29*, 952.
[16] J. Engelke, J. Brandt, C. Barner-Kowollik, A. Lederer, *Polym. Chem.* **2019**, *10*, 3410.
[17] a) A. P. P. Kröger, R. J. E. A. Boonen, J. M. J. Paulusse, *Polymer* **2017**, *120*, 119; b) E. B. Berda, E. J. Foster, E. W. Meijer, *Macromolecules* **2010**, *43*, 1430.
[18] J. Märk, F.-J. Schmitt, C. Theiss, H. Dortay, T. Friedrich, J. Laufer, *Biomed. Opt. Express* **2015**, *6*, 2522.
[19] F.-J. Schmitt, E. G. Maksimov, H. Suedmeyer, V. Jeyasangar, C. Theiss, V. Z. Paschenko, H. J. Eichler, G. Renger, *Photonics Nanostruct. - Fundam. Appl.* **2011**, *9*, 190.
[20] a) J. Märk, F.-J. Schmitt, J. Laufer, *J. Opt.* **2016**, *18*, 54009; b) J. Märk, A. Wagener, E. Zhang, J. Laufer, *Sci. Rep.* **2017**, *7*, 40496; c) F. G. Golmohamadi, A. Mehmood, F.-J. Schmitt, J. Laufer, *Proc. SPIE* **2021**, *11923*, 119230F.
[21] S. Schrof, G. Pang, J. Buchmann, J. Laufer, *J. Imaging* **2018**, *4*, 146.

